catalysts

MDPI

Article

Biogas Upgrading by CO_2 Methanation with Ni-, Ni–Fe-, and Ru-Based Catalysts

Andrés Sanz-Martínez, Paul Durán, Víctor D. Mercader, Eva Francés, José Ángel Peña and Javier Herguido *

Catalysis Molecular Separations and Reactor Engineering Group (CREG), Aragon Institute of Engineering Research (I3A), Universidad Zaragoza, 50018 Zaragoza, Spain
* Correspondence: jhergui@unizar.es

Abstract: This piece of work dealt with the concept of 'biogas upgrading' or enrichment of the CH_4 contained in a sweetened biogas to proportions and features comparable to those of synthetic natural gas (SNG). For this, the behavior of three lab made catalysts (Ni/Al_2O_3, Ru/Al_2O_3, and $Ni–Fe/Al_2O_3$) was tested in a CO_2 methanation reaction (Sabatier reaction) under different feeding conditions (with and without methane). In the first set of experiments (without methane), the good catalytic behavior of the solids was validated. All three catalysts offered similar and increasing CO_2 conversions with increasing temperature (range studied from 250 to 400 °C) at a constant WHSV of 30×10^3 $STPmL \cdot g_{cat}{}^{-1} \cdot h^{-1}$. The CH_4 selectivity remained close to one in all cases. Considering their total metallic load, the Ru (3.7 wt%)-based catalyst stood out remarkably, with TOF values that reached up to 5.1 min^{-1}, this being six or three times higher, than those obtained with the Ni (10.3 wt%) and Ni–Fe (7.4–2.1 wt%) catalysts, respectively. In the second set (cofeeding methane), and also for the three catalysts, a high correspondence between the conversions (and selectivities) obtained with both types of feeds was observed. This indicated that the addition of CH_4 to the system did not severely modify the reaction mechanism, resulting in the possibility of taking advantage of the 'biogas upgrading' process by using H_2 produced off-peak by electrolysis. In order to maximize the CH_4 yield, temperatures in the range from 350–375 °C and a H_2:CO_2 molar ratio of 6:1 were determined as the optimal reaction conditions.

Keywords: methanation; biogas; CO_2; power to gas; Ni–Fe catalysts; Ru catalyst

check for updates

Citation: Sanz-Martínez, A.; Durán, P.; Mercader, V.D.; Francés, E.; Peña, J.Á.; Herguido, J. Biogas Upgrading by CO_2 Methanation with Ni-, Ni–Fe-, and Ru-Based Catalysts. *Catalysts* **2022**, *12*, 1609. https://doi.org/10.3390/catal12121609

Academic Editors: Son Ich Ngo and Enrique García-Bordejé

Received: 4 November 2022
Accepted: 5 December 2022
Published: 8 December 2022

1. Introduction

After repeated attempts of keeping global warming below 2 °C compared to pre-industrial levels [1], the main, perhaps the only, tool to achieve the goal of carbon neutrality by 2050 is a process of energy transition. That is, to abandon the current system of energy based on fossil fuels and make way for a low- or zero-carbon system based on renewable sources. Solar, wind, and geothermal energy are among the best-known renewable energies [2], but they are not the only sources. Other solutions such as those based on biomass have also gained greater importance in recent decades, not only as energy providers but also as waste disposers, with this being a clear exponent of the circular economy paradigm [3,4]. This is so in the case of biogas. This renewable gas is produced by the anaerobic degradation of organic wastes [5]. It is mainly composed of CH_4 (50–70 v%) and CO_2 (30–50 v%) in variable proportions depending on the composition of the organic matter [6]. Other minor compounds such as H_2S, NH_3, or siloxanes must also be considered because they can cause irreparable damage to the process [7].

Biogas can be used in different ways. Although it can be reformed to produce hydrogen (steam, dry, or autothermal reforming), other possibilities seem to be more efficient from an energy point of view. Among them, its combustion to produce electrical and/or thermal energy, or its upgrading to increase its methane content and injecting it into the yet existing natural gas network, seem to be more realistic. Conventional biogas upgrading technologies

are generally based on CO_2 separation (membrane or cryogenic separation, chemical absorption, the pressure swing adsorption (PSA) technique, water scrubbing, etc.), with CO_2 being released into the atmosphere contributing to climate change [8]. An interesting alternative is to carry out the chemical reaction of hydrogenation on the CO_2 contained in the biogas to increase its methane content. Of course, in order to preserve the renewable character of synthetic natural gas (SNG), hydrogen must be produced by electrolysis with surplus electricity of a renewable origin (wind, sun, or tidal in periods of low demand). Another advantage of SNG is that methane, its main constituent, has an energy density three times higher than that of hydrogen, which facilitates its storage and transport [9].

The hydrogenation (or methanation) of CO_2, known as the Sabatier reaction (Equation (1)) [10], is an exothermic reaction thermodynamically favored at high pressures and low temperatures [11]. It can be considered as a series combination of two reactions: the reverse water–gas shift reaction (Equation (2)), which constitutes the partial hydrogenation of CO_2 to give the intermediate product CO, and the CO methanation reaction (or reverse steam reforming) (Equation (3)) to complete the final hydrogenation to CH_4 [12].

$$CO_2 + 4H_2 \rightleftharpoons CH_4 + 2H_2O \quad \Delta H_r^0 = -165.1\ \text{kJ}\cdot\text{mol}^{-1} \tag{1}$$

$$CO_2 + H_2 \rightleftharpoons CO + H_2O \quad \Delta H_r^0 = +41.2\ \text{kJ}\cdot\text{mol}^{-1} \tag{2}$$

$$CO + 3H_2 \rightleftharpoons CH_4 + H_2O \quad \Delta H_r^0 = -206.3\ \text{kJ}\cdot\text{mol}^{-1} \tag{3}$$

Due to kinetic and thermodynamic limitations, the methanation process based on the Sabatier reaction requires the use of supported catalysts. It is known that both noble metals (Ru [13], Rh [14], Pd [15], or Pt [16]) and transition ones (Fe [17], Ni [18], or Co [19]) present catalytic activity in this reaction. Nickel, supported on different metal oxides (mainly alumina), represents the most widely used catalytic system. It has a high activity, good selectivity, and is cheaper that other options [20,21]. The main drawback is that it can be deactivated by coke formation [22] or oxidation of the metal particles [23]; this problem can be partly solved by introducing a second metal such as Fe, Co, Ru, etc. [24]. Ruthenium, in addition to its high activity with low metallic charges [13], has very good selectivity towards CH_4 (even at low temperatures) and high resistance in oxidizing atmospheres [25]. However, its high price makes it difficult to apply on a large scale. Iron has a very low methane selectivity [17], but its addition as promoter with Ni-based catalysts results in a positive effect. Thus, Burger et al. [26] indicated that Fe improves the CO_2 sorption activity and thermal stability of the catalyst (up to temperatures of 500 °C for uninterrupted periods of 32 h). Moghaddam et al. [27] reported that the addition of 5 wt% of a second metal (Fe, Co, Zr, La, or Cu) in catalysts with 30 wt% Ni had the effect of increasing the conversion at low temperatures (especially with Fe). Similar results have been shown by other authors using 25 wt% Ni and 2.5 wt% Fe [28]. Finally, Pandey and Deo [29] reported an increase in the conversion of and selectivity toward CH_4 when a Ni (7.5 wt%) catalyst was doped with Fe (2.5 wt%). In this case, Al_2O_3 was the support that showed the best results [30].

With respect to biogas methanation, the interest generated in recent years by this concept ('biogas upgrading') has resulted in different contributions. Apart from the technical norms concerning the features to be fulfilled by an SNG to be injected in the existing infrastructure for natural gas distribution [31,32], computational studies have shown that direct biogas methanation can produce SNG with adiabatic and cooled reactors [33,34]. These authors also carried out a reliable economic study, indicating that methanation costs are only a minor part of the total budget, but the technical design and uses are very relevant. Boggula et al. [35] report high CH_4 yields in order to satisfy the German gas grid requirements by using a commercial 66 ± 5 wt% Ni on silica–alumina catalyst and a pressure of 10 bar (laboratory-scale experimental setup). The effect of the biogas composition has been considered on a catalyst with over 20 wt% Ni–Mg–Al and different operating conditions [36]. This study concluded that increasing the initial amount of CH_4 present in the biogas decreases the CO_2 conversion but it does not affect the selectivity towards CH_4 (close to 100%). In contrast, Pastor-Pérez et al. [37], using 15 wt% Ni/CeO_2-ZrO_2

catalysts promoted with Co (3 wt%), indicated an increase in both CO_2 conversion and CH_4 selectivity when the initial methane content was increased from 0 to 15 v% in the feed. Compared to the traditional Al_2O_3 support, CeO_2 offers worse catalytic activity results [38]. This research also showed that the introduction of H_2S traces along with the feed stream led to a fast drop in CO_2 conversion and CH_4 selectivity. The presence of CH_4 and H_2S clearly affects the activity of methanation catalysts, but this influence depends on the catalyst composition and reactions conditions [39]. A pilot-scale experimental setup highlighted the importance of controlling the exothermicity of the Sabatier reaction [9,40]. In both cases, the temperature profiles exceeded 200 °C using commercial Ni-based catalysts in a fixed-bed reactor. Other experimental reactor configurations, such as distributed feeding, have been proposed to solve this problem [41].

Considering these premises, the general objective of this work was to study the catalytic methanation of CO_2 (Sabatier reaction) present in a biogas through its upgrading to synthetic natural gas as an alternative to any other kind of use or venting. In order to do this, the use of three catalysts prepared in our laboratory was proposed. These catalysts were based on Ni (10 wt%), Ru (3 wt%), and Ni–Fe (7.5–2.5 wt%), respectively, as the active phases and with alumina as the support. CO_2 methanation (both pure and contained in a synthetic biogas) was tested in a wide range of temperatures (250–400 °C) and in a fixed-bed atmospheric reactor. In the case of synthetic biogas co-feeding, the effect of the partial pressure of reactants (modified by the H_2:CO_2 molar ratio) was also studied.

2. Results and Discussion

2.1. Catalyst Characterization

Table 1 shows the values of the specific surface area (BET method) and chemical composition (XRF) of the prepared catalysts as well as those of the alumina used as catalytic support. A high BET area of the uncalcined Al_2O_3 (200.6 $m^2 \cdot g^{-1}$) was observed. This value decreased with the catalyst impregnation process. The reason was related to the obstruction of part of the Al_2O_3 pores by deposition of the metallic phase (10 wt% Ni, 3 wt% Ru, and 7.5 wt% Ni + 2.5 wt% Fe) on its surface. XRF characterization confirmed the correct preparation of the catalysts in terms of the good correspondence between the nominal and measured metal contents.

Table 1. Surface area (BET) and chemical composition (XRF) of the solids.

Solid	BET Area ($m^2 \cdot g^{-1}$)	XRF (wt%)		
		Ni	Ru	Fe
Al_2O_3	200.6 ± 0.4	-	-	-
10Ni	174.5 ± 0.3	10.3 ± 0.1	-	-
3Ru	190.2 ± 0.6	-	3.7 ± 0.1	-
7.5Ni–2.5Fe	167.4 ± 0.4	7.4 ± 0.1	-	2.1 ± 0.1

XRD characterization was proposed as a complement along with XRF for the identification of the different crystalline phases. The diffractograms ratified the presence of the characteristic peaks of the gamma phase (γ-$Al_{2.1}O_{3.2}$), both in the uncalcined Al_2O_3 and in the prepared catalysts (Figure 1). In the case of the '10Ni' catalyst, other phases coexisted such as NiO or $NiAl_2O_4$ spinel phases. For the '3Ru' catalyst, its corresponding oxide (RuO_2) also appeared. The diffractogram corresponding to the bi-metallic catalyst ('7.5Ni–2.5Fe') showed a negligible signal of the oxidized phase of iron (FeO). This may be due to the low amount of iron impregnated (2.1 wt% according to XRF) and the high dispersion and/or amorphous nature of the deposition of this oxide phase. Other authors have already reported this phenomenon [28,29].

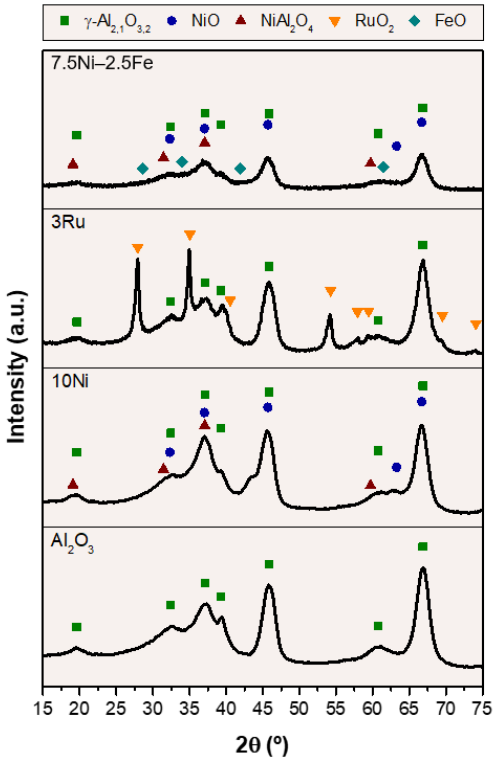

Figure 1. X-ray diffraction patterns of the catalysts and identification of the crystalline phases.

Figure 2 illustrates the reducibility of the different catalysts according to their H_2-TPR characterization. For the '10Ni' catalyst, a broad asymmetric reduction signal ranging from 380 to 700 °C was observed, which was caused by two overlapping reduction peaks centered at 450 and 600 °C. This fact confirmed the presence of different types of nickel oxide.

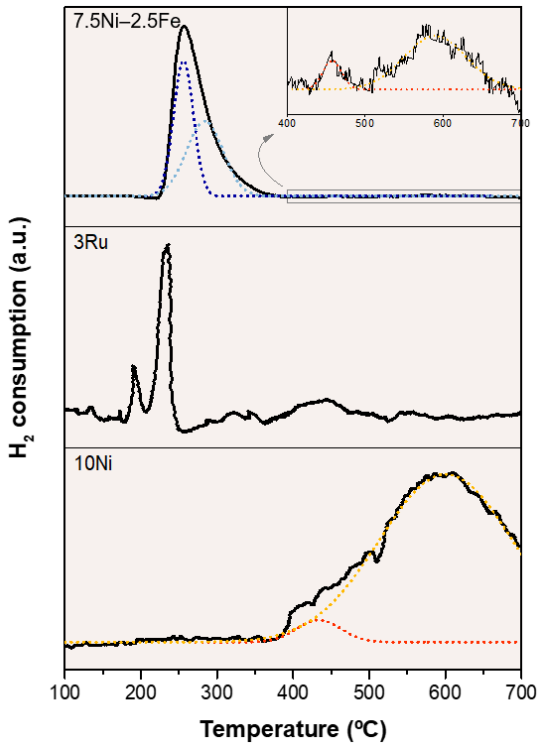

Figure 2. H_2-TPR profiles for the three catalysts. Operating conditions: heating rate β = 2 °C/min (from room temperature to 700 °C), q_0 = 100 STPmL·min^{-1}, v% H_2 = 5% (N_2 balance), and W_{cat} = 0.1 g.

According to Zhou et al. [42], the peak at around 430 °C was attributed to the reduction of NiO to Ni metal, while the one at 600 °C was supposed to be caused by the reduction of NiO that more strongly interacts with Al_2O_3 ('NiO·Al_2O_3', or better described as surface $NiAl_2O_4$). Therefore, the $NiAl_2O_4$ spinel was considered both in the bulk (XRD analysis, Figure 1) and on the catalyst surface. The '3Ru' catalyst showed two main reduction peaks at 190 and 230 °C, which were ascribed to the reduction of RuO_2 to Ru metal. According to Chen et al. [43], the reduction profile corresponded to that reported for ruthenium on alumina catalysts. Initially, the possibility of having more oxidized phases (RuO_3 or RuO_4) was considered. Their non-detection by XRD (Figure 1) ruled out this hypothesis. Finally, for the iron-doped catalyst ('7.5Ni–2.5Fe'), the signals were assigned to the gradual reduction of Fe_2O_3 to Fe. This reduction occurs in the range from 200 to 350 °C. The first peak, centered at 250 °C, corresponded to a first reduction of Fe^{3+} to Fe^{2+}, while the second (275 °C) marked the subsequent reduction of Fe^{2+} to Fe^0 [44]. At higher temperatures, the previously discussed NiO reduction signals appeared, although to a lesser extent (box with enlarged scale).

2.2. CO_2 Methanation

Prior to performing an experimental analysis of the effect of varying the operational conditions (temperature and partial pressures of reactants), a study was carried out with the aim of preserving the results from disturbance by internal or external diffusion limitations. In this sense, experiments were conducted to determine the maximum particle size for the catalyst and the minimum flow rate for the reactants stream. This led to the conditions of particle size and gas flowrate mentioned in the experimental section. In addition, a blank experiment was carried out in absence of catalyst (with only alumina substituting the active species) whilst maintaining the rest of the experimental conditions, which resulted in a null conversion of reactants confirming the inert behavior of the catalyst support.

The effect of temperature on the methanation process of CO_2 was studied in the range from 400–250 °C (in steps of −25 °C at seven temperatures), maintaining each temperature for 60 min. Figure 3 shows the CO_2 and H_2 conversions for a typical experiment as well as the values of equilibrium (dashed horizontal lines) at each temperature, calculated by minimization of the Gibbs free energy $\left(\mathrm{Min}\left\{\frac{\delta(\Delta G)}{\delta n}\right\}\right)$ using the Aspen HYSYS simulation software (SRK as the thermodynamic package). The values of CO_2 conversion shown in Figure 3 were nearly stable along the time-on-stream (at least for every one-hour step) for all the catalysts and temperatures tested, denoting that deactivation by coke formation or other causes was not significant. Under these conditions, the CO_2 conversion and the CH_4 yield led to equivalent values, revealing that no other reactions (including coke formation) apart from Sabatier's (Equation (1)) were significantly present.

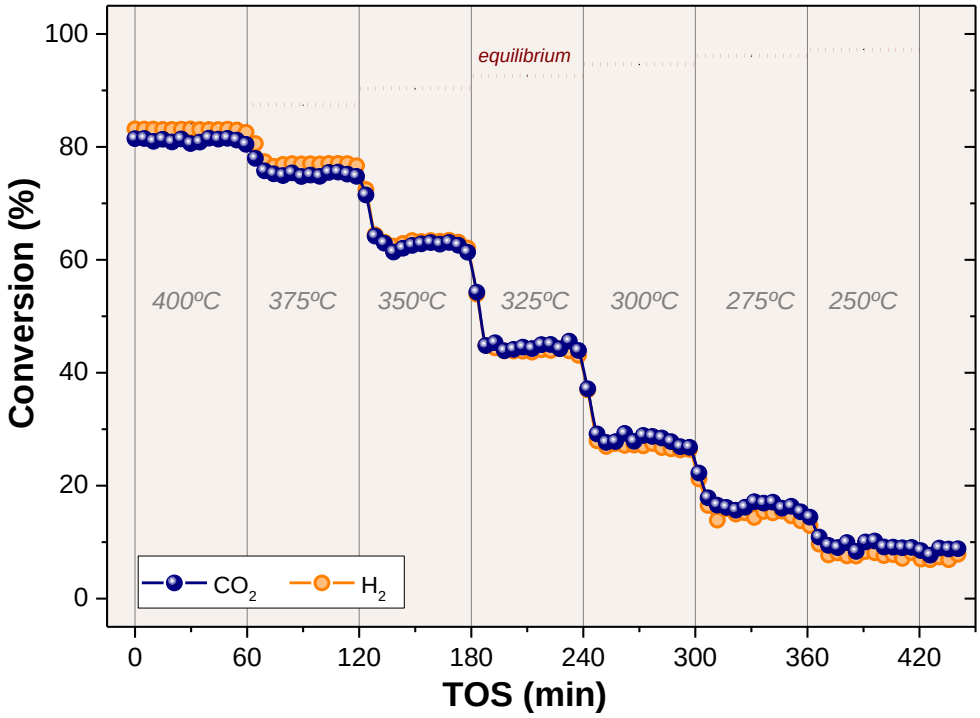

Figure 3. CO_2 and H_2 conversions as a function of temperature and time-on-stream (TOS) for '10Ni' catalyst. Feeding without methane ('W/O CH_4'). Operating conditions (Table 2): q_0 = 250 STPmL·min^{-1}, H_2:CO_2 = 4:1, and WHSV = 30 × 10^3 (STPmL·$g_{cat}{}^{-1}$·h^{-1}).

Table 2. Experimental conditions (base value and studied range) for catalytic activity experiments.

Variable (Units)	Base Value	Studied Range
Catalyst (-)	3Ru	10Ni, 3Ru, 7.5Ni–2.5Fe
T (°C)	-	400–250 *
W_{cat} (g)/W_{inert} (g)	0.5/2.0	-
q_0 (STPmL·min^{-1})	250	-
WHSV (STPmL·$g_{cat}{}^{-1}$·h^{-1})	30,000	-
H_2:CO_2 molar ratio (-)	4:1	2:1, 3:1, 4:1, 5:1, 6:1
CH_4:CO_2 molar ratio ** (-)	7:3	-

* (−25 °C) intervals (seven temperatures). ** only in experiments of biogas methanation.

Figure 4 represents the average CO_2 conversion values for each one-hour step. For all three catalysts, an increase in temperature translated into a clear increase in CO_2 conversion. The largest conversion increase occurred in the low–medium temperature range (250 to 325 °C). This behavior confirmed that for the operating WHSV (30 × 10^3 STPmL·$g_{cat}{}^{-1}$·h^{-1}), the system was far from its thermodynamic equilibrium. It was the reaction kinetics that determined the conversion achieved. Only at the highest temperatures (375 and 400 °C) did the experimental values approach those of equilibrium. In all cases, the selectivity to CH_4 (Equation (3)) was very close to 100%. Other possible gaseous by-products such as CO were not detected (detection limit of the analysis system in the range of 50 ppm).

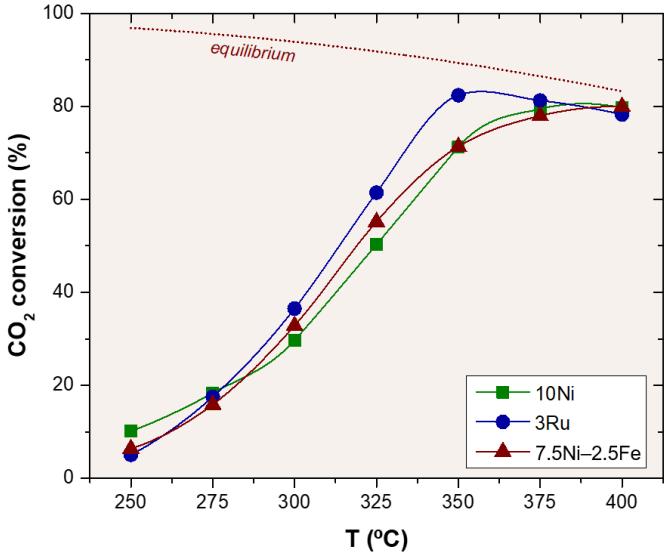

Figure 4. CO_2 conversion as a function of temperature and catalyst tested for a feed without methane ('W/O CH_4'). Operating conditions (Table 2): q_0 = 250 STPmL·min^{-1}, H_2:CO_2 = 4:1, and WHSV = 30 × 10^3 (STPmL·$g_{cat}{}^{-1}$·h^{-1}). Lines are only for visual help. Dashed curve represents thermodynamic equilibrium.

In the case of the '10Ni' and '7.5Ni–2.5Fe' catalysts, the maximum CO_2 conversion temperature was achieved at 400 °C, while for the '3Ru' catalyst it was 350 °C (Figure 4). In this figure, the CO_2 conversions were similar for the three catalysts. Only for the temperature range from 325–375 °C did the '3Ru' catalyst exceed the '10Ni' or '7.5Ni–2.5Fe' ones. At the working WHSV, the higher activity of the Ru-based catalyst allowed approaching equilibrium at a lower temperature (around 350 °C) than the other two solids. Consequently, above 350 °C, the higher the temperature, the lower the conversion using this catalyst.

In terms of TOF (Equation (7)), the differences between the catalysts were much greater (Figure 5). The lower metallic load of the Ru-based catalyst (3.7 wt%, see Table 1) compared to the Ni-based (10.3 wt%) or Ni–Fe-based (7.4–2.1 wt%) catalysts, implied TOF values that reached almost six times (5.8) or three times (3.0) those obtained at 350 °C, respectively. For the full range of temperatures (250–400 °C), this difference represented a factor of 5.3 for the comparison of '3Ru' vs. '10Ni' and 3.3 for that of '3Ru' vs. '7.5Ni–2.5Fe'.

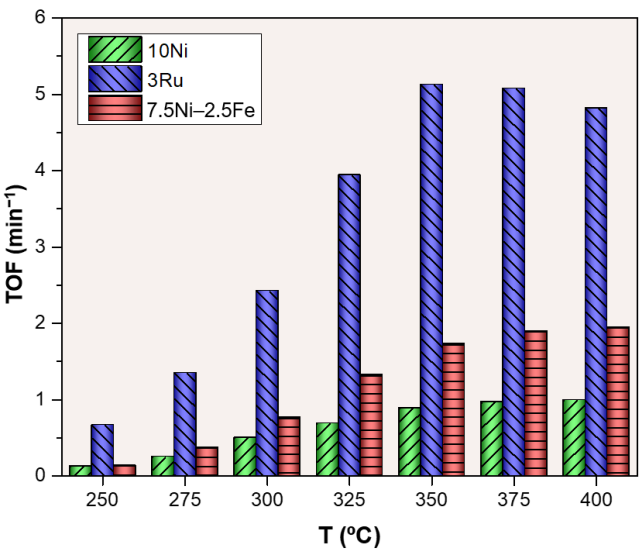

Figure 5. Comparison of specific activity of three catalysts tested ('W/O CH_4') in terms of TOF (Equation (7)). Operating conditions: same as in Figure 4.

The following ranking of catalysts was established according to their activity (TOF terms) in the CO_2 methanation process: '3Ru' > '7.5NiFe' > '10Ni'. This classification justified the preselection of the '3Ru' catalyst to carry out the study of varying the H_2:CO_2 molar ratio in the subsequent section.

2.3. Biogas Methanation

As an additional aspect to the previously shown CO_2 methanation experiments, the behavior of the three catalysts was evaluated when the feed incorporated CH_4. This would be the case in the event of sweetened biogas upgrading, in which CO_2 present in the biogas (previously desulfurized) is forced to react with H_2 to increase the CH_4 content following the reaction (Equation (1)).

Figure 6 shows the comparison of the CO_2 conversion values (Equation (1)) obtained for the three catalysts at different temperatures when using both types of feeding: without methane ('W/O CH_4') and with methane in its composition ('Biogas'). Note that the H_2:CO_2 molar ratio was always kept at 4:1. Additionally, in the case of methane co-feeding, the CH_4:CO_2 molar ratio was always adjusted to 7:3; thus, the simulated 'Biogas' with simultaneous feeding of H_2 presented a CH_4:H_2:CO_2 molar ratio of 7:12:3.

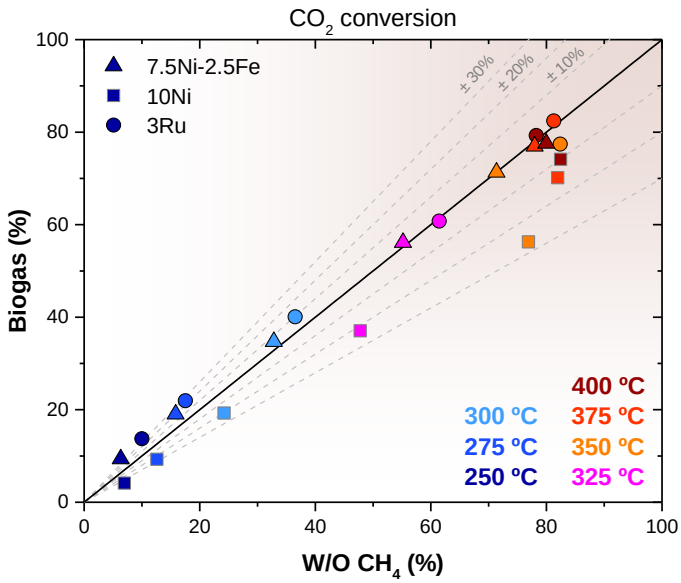

Figure 6. Influence on CO_2 conversion of co-feeding methane ('Biogas' vs. 'W/O CH_4') for all catalysts and different temperatures. Operating conditions (Table 2): q_0 = 250 STPmL·min^{-1}, H_2:CO_2 = 4:1, CH_4:CO_2= 7:3, and WHSV = 30 × 10^3 (STPmL·$g_{cat}{}^{-1}$·h^{-1}).

These results indicated that the agreement between both processes of methanation ('W/O CH_4' and 'Biogas') was high in general terms, with CO_2 conversion values distributed mostly along the main diagonal of the parity plot (Figure 6). However, in the specific case of the '10Ni' catalyst, a more pronounced deviation was observed, and at all temperatures, lower CO_2 conversions were obtained when CH_4 was co-fed (i.e., for the 'W/O CH_4' feed). In this same sense, Jürgensen et al. [45], carrying out some equilibrium simulations, predicted a significant effect of the methane content in the biogas feed stream on CO_2 conversion when working at low pressures. Additionally, taking as reference the experimental work by Han et al. [36] with a Ni–Mg–Al catalyst at 400 °C and H_2:CO_2 = 4:1, a decrease in CO_2 conversion of around 9% was derived when the content of CH_4 in their reactant gas was similar to the one used here (around 30%) compared to that in the absence of CH_4. Thus, the '10Ni' catalyst aligned with this behavior, also agreeing with Le Chatêlier's principle, showing a nearly identical conversion decrease at 400 °C (Figure 6) and an even sharper decrease at lower temperatures.

Unlike the '10Ni' catalyst, for the '3Ru' and '7.5Ni–2.5Fe' catalysts, similar or even slightly higher CO_2 conversions were distinguished in the case of co-feeding methane (the 'Biogas' cases). In fact, in the low–medium temperature zone interval (250 to 325 °C), the behavior seemed to be reversed (slightly higher conversions for a feed based on biogas), adopting a contrary trend to Le Chatêlier's principle. Pastor-Pérez et al. [37] also found this beneficial effect caused by the presence of methane on the catalytic performance in the methanation reaction using a Ni (15 wt%)–Co (3.5 wt%)/CeO_2-ZrO_2 catalyst and working under similar conditions to those of this work. They explained the increase in CO_2 consumption by two different causes: (i) the promotion of reforming reactions at relatively low temperatures by the extra methane fed and (ii) the presence of extra hydrogen on the catalyst surface from the decomposition of methane, which favors the CO_2 methanation.

Cárdenas-Arenas et al. [46] recently reported that with Ni/Al_2O_3 catalysts, hydrogen reduces NiO-Al_2O_3 species creating hydroxyl groups where CO_2 is chemisorbed and dissociated. Then, they yield formates and water. Finally, part of these formates can be hydrogenated to give methane or alternatively be decomposed to give CO. However, for Ni-based bimetallic catalysts (such as FeNi) or Ru-based ones, the higher CH_4 yields obtained with them are attributed [24] to a different surface reaction mechanism involving the creation of suitable sites (FeO_x or dispersed Ru^0) that can potentially favor CO_2 chemisorption and activation. The different behavior found, in terms of CO_2 conversion (Figure 6), between '10Ni' on the one hand and '7.5Ni–2.5Fe' or '3Ru' on the other could be attributed to these different surface reaction mechanisms

The effect of temperature observed for these experimental series was preserved with respect to that presented for CO_2 methanation: an increase in temperature produced an increase in conversion, except for the '3Ru' catalyst, for which the maximum was at 350 °C. The distribution of products (not shown) also did not change between both types of feeds, reporting CH_4 selectivities close to 100%. Likewise, as in Figure 3, the three catalysts showed stable behavior during the hour of operation during which each temperature was maintained.

It was concluded that, although it slightly varied with the specific catalyst, the effect of including a certain proportion of CH_4 in the feed (in addition to H_2 and CO_2) was not negative for the process under the conditions tested. This opens an interesting perspective for the applicability of the 'biogas upgrading' concept or the enrichment of the methane contained in a biogas (e.g., that produced in landfills) to achieve a composition similar to that of natural gas, which eventually, fulfilling all the specifications imposed by technical norms, can be reinjected in the natural gas network.

Finally, different H_2:CO_2 molar ratios (from 2:1 to 6:1) were tested for the catalyst based on ruthenium ('3Ru'), which was the most active one among those preselected. Thus, the effect of the partial pressure of reagents (in addition to temperature) was also considered. This study was also carried out both for a feed without methane ('W/O CH_4') and for one that simulated a desulfurized biogas as a source of CO_2 ('Biogas'). In all cases, the weight hourly space velocity (q_0/W_{cat}) was kept constant at the base value (30×10^3 STPmL·$g_{cat}{}^{-1}$·h^{-1}). Figure 7 shows the parity plot comparing both feeds.

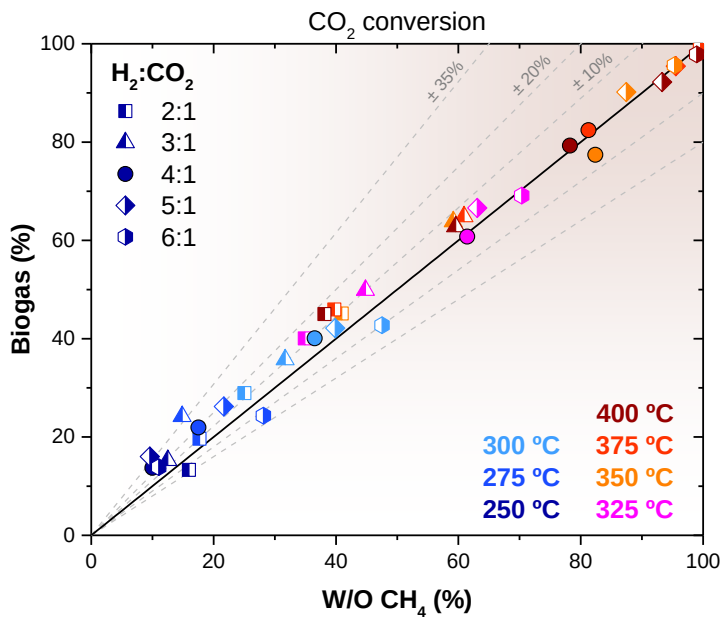

Figure 7. Influence of methane co-feeding on CO_2 conversion ('Biogas' vs. 'W/O CH_4') for '3Ru' catalyst at different temperatures and H_2:CO_2 molar ratios. Operating conditions (Table 2): q_0 = 250 STPmL·min^{-1}, H_2:CO_2 = 4:1, CH_4:CO_2= 7:3, and WHSV = 30 × 10^3 (STPmL·$g_{cat}{}^{-1}$·h^{-1}).

It was observed how the agreement between CO_2 conversion for both feeds was maintained for the entire range of temperatures (250–400 °C) and H_2:CO_2 molar ratios (2:1–6:1). This reaffirmed the hypothesis raised in this research, by which a feeding stream rich in CH_4 did not have any significant adverse effect, resulting in the possibility of using a sweetened biogas as a very promising alternative to be upgraded. In fact, with this specific ruthenium-based catalyst ('3Ru') and the operating conditions tested, the predominant effect was beneficial when CH_4 was co-fed (Figure 7).

The increase in conversion with temperature was also maintained with respect to the previous operations. From 375 °C (or 350 °C, depending on the H_2:CO_2 molar ratio), this conversion began to decrease due to the limits imposed by thermodynamics. Regarding the effect of the molar ratio of reactants, a higher H_2:CO_2 ratio, and consequently a lower proportion of CO_2, translated into an increase in its conversion. This phenomenon was justified by attending to the excess (or deficiency) of the reactant, CO_2, with respect to H_2, as predicted by the Sabatier reaction (Equation (1)). A complete selectivity toward CH_4 and stable operation for all the H_2:CO_2 ratios studied along the hour that the reaction was maintained at each temperature was reported, as shown in Figure 3.

The CH_4 yield curves (not shown) presented a behavior equivalent to that of the CO_2 conversion (previously represented in Figure 7). An increase in temperature translated into an increase in the CH_4 yield. The CO_2 partial pressure had the opposite effect: at an equal temperature, the higher the H_2:CO_2 molar ratio (i.e., the lower the CO_2 partial pressure), the greater the CH_4 yield. Even though the reactor was always operated at a constant WHSV of 30 × 10^3 STPmL·$g_{cat}{}^{-1}$·h^{-1}, the specific value of space velocity related to CO_2 varied with each H_2:CO_2 molar ratio, proportionally decreasing from 9.0 × 10^3 to 3.9 × 10^3 STPmL$_{CO2}$·$g_{cat}{}^{-1}$·h^{-1} when the H_2:CO_2 ratio changed from 2:1 to 6:1. The subsequent increase in $W_{cat}/f^{wt}_{0,\,CO_2}$ (from 5.6 × 10^{-2} h to 13.2 × 10^{-2} h) produced an improvement in CO_2 conversion and consequently in the CH_4 yield. Therefore, it was understandable to relate the positive effect of operating at high H_2:CO_2 molar ratios on the CH_4 yield [36]. These results were consistent with a series–parallel reaction scheme, in which H_2 acted as an attacking reagent on CO_2 in two consecutive stages: a reverse water–gas shift reaction—rWGS—(Equation (2)) and a reverse methane steam-reforming reaction—rMSR—(Equation (3)) [41].

3. Materials and Methods

3.1. Preparation and Characterization of Catalysts

Three supported solid catalysts were prepared. The first two (monometallic) used Ni (10 wt%) or Ru (3 wt%) as the active phase. The third one was based on a Ni–Fe combination (7.5–2.5 wt%). As the catalytic support, γ-Al_2O_3 (Puralox SCCa-150/200, Sasol, Hamburg, Germany) was used in all cases. The catalysts were prepared by the incipient wetness impregnation method (at room temperature) from the commercial metal precursors (Sigma Aldrich, St Louis, Mo, U.S.) $Ni(NO_3)_3{\cdot}6H_2O$ (98.6%), $RuCl_3{\cdot}3H_2O$ (Ru = 41.12%), and $Fe(NO_3)_3{\cdot}9H_2O$ ($\geq$98.0%). For the bimetallic catalyst, the impregnation of Ni and Fe precursor solutions was performed simultaneously. After drying (120 °C, for 12 h), the samples were calcined (B180, Nabertherm, Lilienthal, Germany) in air (500 °C with a heating rate of 5 °C/min for 8 h). Then, they were crushed and sieved to the working particle diameter (100–250 μm). Before their use in the reaction, the catalysts were activated as indicated in the following section. The three catalysts were labelled as '10Ni', '3Ru', and '7.5Ni–2.5Fe' according to their respective nominal mass percentage of metal or combination of them in the whole sample.

The specific surface area (BET) of the prepared catalysts and plain alumina (support) was characterized by N_2 physical adsorption at −196 °C (Tristar 3000 V6.08, Micromeritics, Norcross, GA, U.S.). Prior to measurements, samples were degassed at 200 °C (VacPrep 061, Micromeritics, Norcross, GA, U.S.). X-ray fluorescence (XRF) was performed to determine the metal content. The equipment employed was a sequential spectrometer (ARL ADVANT'X, Thermo Electron, Waltham, MA, USA), which used a Rh X-ray tube. The UniQuant 5.0 software was employed for the semiquantitative analysis without standards (sequential analysis from Mg to U). The structural analysis of crystalline species was determined by X-ray diffraction (XRD) (Max-System, Rigaku, Wilmington, MA, USA, equipped with a Cu-anode). Data acquisition was carried out with a 2θ range from 5 to 90° and a step of 0.03°. A graphite monochromator was used for the selection of CuKα radiation from the anode (λ = 1.5418 Å). Finally, temperature-programmed reductions with H_2 measurements (H_2-TPR) were performed on the three catalysts in order to determine their effective reduction temperature. A 5 v% H_2-in-N_2 mixture was fed to a fixed bed reactor (0.1 g of sample) with a total flow rate of 100 STPmL·min^{-1} and under a heating rate of 2 °C/min (from room temperature to 700 °C). Hydrogen consumption was analyzed at the outlet of the sample holder and compared with that of the feed (TCD signal).

3.2. Catalytic Activity Experiments

The reaction system was based on a quartz-made cylindrical fixed bed reactor (i.d. 13 mm and 500 mm height). This reactor was placed in a vertical position inside an electric furnace (1.5 kW_e). The reaction temperature was measured by a K-type thermocouple (centered inside the catalyst bed), which was connected to a PID controller (3116, Eurotherm, Worthing, West Sussex, England). A porous quartz plate with pores smaller than 90 μm supported the catalyst bed and acted as a gas distributor. Gases were fed (top-down) using mass-flow controllers (Alicat Scientific, Tucson, AZ, USA). Exhaust gases were analyzed with a micro-gas chromatograph (490 Micro-GC, Agilent Technologies, Santa Clara, CA, USA) after the separation of condensed liquids (mainly water) by a cold trap (Peltier module) that operated at ca. 4 °C and at atmospheric pressure. The Micro-GC device was equipped with two molecular sieves (10 m MS-5A) (Ar and He as the carrier gases, respectively) and a capillary column (10 m PPQ). MS-5A was used to detect permanent gases (H_2, N_2, CH_4, and CO) while PPQ did the same for CO_2. The sampling frequency was approximately 6.5 min.

The catalytic activity experiments were classified into two groups depending on the type of feed. In the first set (CO_2 methanation), the feed consisted exclusively of CO_2 and H_2 as the reactive species. The molar ratio of H_2:CO_2 was always fixed to 4:1 according to the stoichiometric proportion given by the Sabatier reaction (Equation (1)). These experiments were labeled as 'W/O CH_4' in the figures to come.

In the second set (*biogas methanation*), a stream of CO_2 and CH_4 simulating a sweetened biogas was chosen as CO_2 source. Its composition was maintained at a CH_4:CO_2 molar ratio of 7:3, which is typical of biogas obtained by the anaerobic degradation of organic matter [6]. These experiments were labeled as 'Biogas'. The mass of catalyst load (W_{cat} = 0.5 g) and the total feed flow rate (q_0 = 250 STPmL·min^{-1}) were kept at a constant value (Table 2) corresponding to a space-time (W_{cat}/q_0) of 20 × 10^{-4} g_{cat}·min·STPmL^{-1} (i.e., WHSV of 30 × 10^3 STPmL·$g_{cat}{}^{-1}$·min^{-1}). N_2 (0.05 bar) was added as an internal standard and Ar (0.05) was added as an inert to complete atmospheric pressure. γ-Al_2O_3 of the same particle diameter as the catalyst (100–250 µm) was used as an inert solid in the bed for heat dilution purposes. The range of temperatures studied was from 400 °C to 250 °C (in steps of −25 °C), with each temperature maintained for 60 min. In the biogas methanation experiments, the effect of the partial pressure of reagents (H_2:CO_2 molar ratio varied from 2:1 to 6:1) was also studied for the ruthenium-based catalyst. The stoichiometric ratio (H_2:CO_2 = 4:1) predicted by the Sabatier reaction (Equation (1)) was always taken as a reference.

The different parameters evaluated to measure the catalytic activity were CO_2 conversion (Equation (4)), CH_4 yield (Equation (5)), CH_4 selectivity (Equation (6)), and turn-over frequency (TOF) (Equation (7)). TOF was referred to the metal content (Ni, Fe, or Ni + Fe) according to the XRF characterization measured values as opposed to nominal ones.

$$CO_2 \text{ conversion } (\%) = \left[\frac{f_{CO_2}|_{In} - f_{CO_2}|_{Out}}{f_{CO_2}|_{In}}\right] \times 100 \quad (4)$$

$$CH_4 \text{ yield } (\%) = \left[\frac{f_{CH_4}|_{Out} - f_{CH_4}|_{In}}{f_{CO_2}|_{In}}\right] \times 100 \quad (5)$$

$$CH_4 \text{ selectivity } (\%) = \left[\frac{f_{CH_4}|_{Out} - f_{CH_4}|_{In}}{f_{CO_2}|_{In} - f_{CO_2}|_{Out}}\right] \times 100 \quad (6)$$

$$\text{TOF } \left(\text{min}^{-1}\right) = \frac{f_{CH_4}|_{Out} - f_{CH_4}|_{In}}{W_{cat} \times 10 \times \left(\frac{wt\%}{M_W}\right)_{metal}} \quad (7)$$

where $f_k|_{In}$ represents the molar flow (mmol·min^{-1}) of compound 'k' being fed into the system, $f_k|_{Out}$ is the molar flow (mmol·min^{-1}) of 'k' in the outlet stream, W_{cat} is the catalyst load (g), wt% is the metal content in the catalyst according XRF measurements (%), and M_w is the molar weight of the active species (g mol^{-1}). In all cases, the corresponding atomic closure balances were established with experimental errors below 5%.

Before the experimental runs, the catalysts were reduced in the same reactor and with the same total flow rate as that used in reaction. The '10Ni' and '7.5Ni–2.5Fe' catalysts were activated with a 50 v% H_2/N_2 mixture (500 °C for 2 h). For the '3Ru' catalyst, it was decided to implement an in situ activation using the conventional feed (400 °C for 2 h). This method was called 'reactive activation', since fresh catalyst was activated alongside time under the same atmosphere used in the kinetic experiments. This phenomenon was probably due to the redispersion of Ru on the surface of the catalyst [47,48].

4. Conclusions

The efficacy of the studied catalysts ('10Ni', '3Ru', and '7.5Ni–2.5Fe') for biogas upgrading, i.e., increasing the CH_4 concentration through the Sabatier reaction, was demonstrated for a representative synthetic biogas (70 v% CH_4 and 30 v% CO_2). The catalyst characterization results (BET, XRF, XRD, and H_2-TPR) showed the proper concentration of each active species, keeping a high specific surface area (provided by their support of gamma alumina). Thus, incipient wetness impregnation was validated as an appropriated synthesis method.

For the experiments only feeding H_2 and CO_2, all the catalysts tested presented similar CO_2 conversions. However, the Ru-based catalyst exhibited slightly higher (ca. 15%) CO_2 conversions from 325 to 375 °C. In terms of TOF (referred to the mass of total active phase),

the positive intensification effect of combining Fe with Ni was clear. The TOF comparison ratio for Ru vs. Ni presented a value of 5.3, and the value was 3.3 for Ru vs. Ni–Fe. Furthermore, the CH_4 selectivities remained close to unity in all cases, indicating a low (or even null) formation of by-products such as CO or CH_3OH.

Equilibrium for the CO_2 conversion was not reached with the experimental space time, approaching it only at the highest temperatures (375–400 °C). The methanation experiments were surely controlled by their kinetics. Therefore, an increase in temperature translated in all cases into an increase in conversion. Finally, a decrease in the CO_2 partial pressure (increasing the H_2:CO_2 molar ratio) translated into increasing the CO_2 conversions and CH_4 yields.

The presence of methane in the feed stream (biogas methanation experiments) had no significant adverse effect on the process. Performance factors such as reactant conversion, CH_4 selectivity, and stability remained essentially unaltered as compared to those of the methane-free feed. Only for some cases, specifically when using the '10Ni' catalyst in the temperature range from 325 to 400 °C, did the CO_2 conversion worsen noticeably when co-feeding methane. Even though its presence decreased the partial pressure of the reactants and consequently the reaction kinetics, and it should also promote the reverse of the Sabatier reaction (Le Chatêlier's principle), these adverse effects were apparently counteracted when using the catalysts with a higher specific activity ('3Ru' and '7.5Ni–2.5Fe', Figure 5). Indeed, a pseudo-inert role of methane in the process could be claimed for those catalysts. This highlights their use for biogas upgrading under the power to gas strategy.

Author Contributions: Conceptualization, E.F., J.Á.P. and J.H.; data curation, A.S.-M. and P.D.; methodology, P.D., J.Á.P. and J.H.; supervision, E.F., J.Á.P. and J.H.; validation, A.S.-M., P.D. and V.D.M.; writing—original draft, A.S.-M.; writing—review & editing, P.D., E.F., J.Á.P. and J.H. All authors have read and agreed to the published version of the manuscript.

Funding: This research was funded by MINECO (Spanish Ministerio de Economía y Competitividad), project number CTQ2016-77277-R, and MICINN (Ministerio de Ciencia e Innovación), project number PID2019-104866RB-I00. In addition, the consolidated research Catalysis, Molecular Separations and Reactor Engineering Group (CREG) had the financial support of Gobierno de Aragón (Aragón, Spain) through European Social Fund—FEDER.

Data Availability Statement: Not applicable.

Acknowledgments: Authors would like to acknowledge the use of Servicio General de Apoyo a la Investigación-SAI (Universidad de Zaragoza).

Conflicts of Interest: The authors declare no conflict of interest.

References

1. United Nations. The Paris Agreement. 2015. Available online: https://unfccc.int/process/conferences/pastconferences/paris-climate-change-conference-november-2015/paris-agreement (accessed on 10 March 2022).
2. Gielen, D.; Boshell, F.; Saygin, D.; Bazilian, M.D.; Wagner, N.; Gorini, R. The role of renewable energy in the global energy transformation. *Energy Strategy Rev.* **2019**, *24*, 38–50. [CrossRef]
3. Conti, C.; Mancusi, M.L.; Sanna-Randaccio, F.; Sestini, R.; Verdolini, E. Transition towards a green economy in Europe: Innovation and knowledge integration in the renewable energy sector. *Res. Policy* **2018**, *47*, 1996–2009. [CrossRef]
4. European Commission. *Communication from the Commission: The European Green Deal*; COM: Brussels, Belgium, 2019. Available online: https://eur-lex.europa.eu/legal-content/EN/TXT/?uri=CELEX:52019DC0640 (accessed on 10 March 2022).
5. Korberg, A.D.; Skov, I.R.; Mathiesen, B.V. The role of biogas and biogas-derived fuels in a 100% renewable energy system in Denmark. *Energy* **2020**, *199*, 117426. [CrossRef]
6. Angelidaki, I.; Treu, L.; Tsapekos, P.; Luo, G.; Campanaro, S.; Wenzel, H.; Kougias, P.G. Biogas upgrading and utilization: Current status and perspectives. *Biotechnol. Adv.* **2018**, *36*, 452–466. [CrossRef] [PubMed]
7. Calbry-Muzyka, A.S.; Gantenbein, A.; Schneebeli, J.; Frei, A.; Knorpp, A.J.; Schildhauer, T.J.; Biollaz, S.M.A. Deep removal of sulfur and trace organic compounds from biogas to protect a catalytic methanation reactor. *Chem. Eng. J.* **2019**, *360*, 577–590. [CrossRef]
8. Zhao, J.; Li, Y.; Dong, R. Recent progress towards in-situ biogas upgrading technologies. *Sci. Total Environ.* **2021**, *800*, 149667. [CrossRef]

9. Dannesboe, C.; Hansen, J.B.; Johannsen, I. Catalytic methanation of CO_2 in biogas: Experimental results from a reactor at full scale. *React. Chem. Eng.* **2020**, *5*, 183–189. [CrossRef]
10. Sabatier, P.; Senderens, J.B. New methane synthesis. *Compt. Rend. Acad. Sci.* **1902**, *134*, 514–516.
11. Gao, J.; Wang, Y.; Ping, Y.; Hu, D.; Xu, G.; Gu, F.; Su, F. A thermodynamic analysis of methanation reactions of carbon oxides for the production of synthetic natural gas. *RSC Adv.* **2012**, *2*, 2358–2368. [CrossRef]
12. Saeidi, S.; Najari, S.; Fazlollahi, F.; Nikoo, M.K.; Sefidkon, F.; Klemes, J.J.; Baxter, L.L. Mechanisms and kinetics of CO_2 hydrogenation to value-added products: A detailed review on current status and future trends. *Renew. Sustain. Energy Rev.* **2017**, *80*, 1292–1311. [CrossRef]
13. Zhuang, Y.; Simakov, D.S.A. Single-pass conversion of CO_2/CH_4 mixtures over the low-loading Ru/γ-Al_2O_3 for direct biogas upgrading into renewable natural gas. *Energy Fuels* **2021**, *35*, 10062–10074. [CrossRef]
14. Karelovic, A.; Ruiz, P. CO_2 hydrogenation at low temperature over Rh/γ-Al_2O_3 catalysts: Effect of the metal particle size on catalytic performances and reaction mechanism. *Appl. Catal. B Environ* **2012**, *113–114*, 237–249. [CrossRef]
15. Martins, J.; Batail, N.; Silva, S.; Rafik-Clemnent, S.; Karelovic, A.; Debecker, D.P.; Chaumonnot, A.; Uzio, D. CO_2 hydrogenation with shape-controlled Pd nanoparticles embedded in mesoporous silica: Elucidating stability and selectivity issues. *Catal. Commun.* **2015**, *58*, 11–15. [CrossRef]
16. Yu, K.P.; Yu, W.Y.; Kuo, M.C.; Liou, Y.C.; Chien, S.H. Pt/titania-nanotube: A potential catalyst for CO_2 adsorption and hydrogenation. *Appl. Catal. B Environ.* **2008**, *84*, 112–118. [CrossRef]
17. Kirchner, J.; Anolleck, J.K.; Lösch, H.; Kureti, S. Methanation of CO_2 on iron based catalyst. *Appl.Catal. B Environ.* **2018**, *223*, 47–59. [CrossRef]
18. Guo, X.; Traitagwong, A.; Hu, M.; Zuo, C.; Meeyoo, V.; Peng, Z.; Li, C. Carbon dioxide methanation over nickel-based catalysts supported on various mesoporous material. *Energy Fuels* **2018**, *32*, 3681–3689. [CrossRef]
19. Zhang, Z.; Zhang, X.; Zhang, L.; Gao, J.; Shao, Y.; Dong, D.; Zhang, S.; Liu, Q.; Xu, L.; Hu, X. Impacts of alkali or alkaline earth metals addition on reaction intermediates formed in methanation of CO_2 over cobalt catalysts. *J. Energy Inst.* **2020**, *93*, 1581–1596. [CrossRef]
20. Jaffar, M.M.; Nahil, M.A.; Williams, P.T. Parametric study of CO_2 methanation for Synthetic Natural Gas production. *Energy Technol.* **2019**, *7*, 1900795. [CrossRef]
21. Tan, C.H.; Nomanbhay, S.; Shamsuddin, A.; Park, Y.-K.; Hernándes-Cocoletzi, H.; Show, P.L. Current developments in catalytic methnation of carbon dioxide-A review. *Front. Energy Res.* **2022**, *9*, 795423. [CrossRef]
22. Liu, Q.; Gu, F.; Gao, J.; Li, H.; Xu, G.; Su, F. Coking-resistant Ni-ZrO_2/Al_2O_3 catalyst for CO methanation. *J. Energy Chem.* **2014**, *23*, 761–770. [CrossRef]
23. Mutz, B.; Belimov, M.; Wang, W.; Sprenger, P.; Serrer, M.A.; Wang, D.; Pfeifer, P.; Kleist, W.; Grunwaldt, J.D. Potential of an alumina-supported Ni_3Fe catalyst in the methanation of CO_2: Impact of alloy formation on activity and stability. *ACS Catal.* **2017**, *7*, 6802–6814. [CrossRef]
24. Tsitsias, A.I.; Charisiou, N.D.; Yentekakis, I.V.; Goula, M.A. Bimetallic Ni-based catalysts for CO_2 methanation: A review. *Nanomaterials* **2021**, *11*, 28. [CrossRef] [PubMed]
25. Hu, J.; Brooks, K.P.; Holladay, J.D.; Howe, D.T.; Simon, T.M. Catalyst development for microchannel reactors for martian in situ propellant production. *Catal. Today* **2007**, *125*, 103–110. [CrossRef]
26. Burger, T.; Koschany, F.; Thomys, O.; Köhler, K.; Hinrichsen, O. CO_2 methanation over Fe- and Mn-promoted co-precipitated Ni-Al catalysts: Synthesis, characterization and catalysis study. *Appl. Catal. A Gen.* **2018**, *558*, 44–54. [CrossRef]
27. Moghaddam, S.V.; Rezaei, M.; Meshkani, F.; Daroughegi, R. Carbon dioxide methanation over Ni-M/Al_2O_3 (M: Fe, Co, Zr, La and Cu) catalysts synthesized using the one-pot sol-gel synthesis method. *Int. J. Hydrogen Energy* **2018**, *43*, 16522–16533. [CrossRef]
28. Mebrahtu, C.; Abate, S.; Chen, S.; Sierra, A.F.; Perathoner, S.; Krebs, F.; Palkovits, R.; Centi, G. Enhanced catalytic activity of iron-promoted nickel on γ-Al_2O_3 nanosheets for carbon dioxide methanation. *Energy Technol.* **2018**, *6*, 1196–1207. [CrossRef]
29. Pandey, D.; Deo, G. Effect of support on the catalytic activity of supported Ni–Fe catalysts for CO_2 methanation reaction. *J. Ind. Eng. Chem.* **2016**, *33*, 99–107. [CrossRef]
30. Wang, X.; Jin, R.; Yan, W.; Li, H.; Wang, Z.-j. An Al_2O_3-supported NiFe bimetallic catalyst derived from hydrotalcite precursors for efficient CO_2 methanation. *Catal. Today.* **2022**, *402*, 38–44. [CrossRef]
31. US EPA. *An Overview of Renewable Natural Gas from Biogas*; EPA 456-R-20-001: Washington, DC, USA, 2020. Available online: https://www.epa.gov/sites/default/files/2020-07/documents/lmop_rng_document.pdf (accessed on 10 March 2022).
32. *ISO 13686*; Natural Gas–Quality Designation. International Organization for Standardization: Geneva, Switzerland, 2013.
33. Gutiérrez-Martín, F.; Rodríguez-Antón, L.M.; Legrand, M. Renewable power-to-gas by direct catalytic methanation of biogas. *Renew. Energy* **2020**, *162*, 948–959. [CrossRef]
34. Canu, P.; Pagin, M. Biogas upgrading by 2-steps methanation of its CO_2-thermodynamics analysis. *J. CO2 Util.* **2022**, *63*, 102123. [CrossRef]
35. Boggula, R.R.; Fischer, D.; Casaretto, R.; Born, J. Methanation potential: Suitable catalyst and optimized process conditions for upgrading biogas to reach gas grid requirements. *Biomass Bioenergy* **2020**, *133*, 105447–105454. [CrossRef]
36. Han, D.; Kim, Y.; Byun, H.; Cho, W.; Baek, Y. CO_2 methanation of biogas over 20 wt% Ni-Mg-Al catalyst: On the effect of N_2, CH_4, and O_2 on CO_2 conversion rate. *Catalysts* **2020**, *10*, 1201. [CrossRef]

37. Pastor-Pérez, L.; Patel, V.; Le Saché, E.; Reina, T.R. CO_2 methanation in the presence of methane: Catalysts design and effect of methane concentration in the reaction mixture. *J. Energy Inst.* **2020**, *93*, 415–424. [CrossRef]
38. Gac, W.; Zawadzki, W.; Rotko, M.; Greluk, M.; Slowik, G.; Pennemann, H.; Neuberg, S.; Zapf, R.; Kolb, G. Direct conversion of carbon dioxide to methane over ceria- and alumina-supported nickel catalysts for biogas valorization. *Chempluschem* **2021**, *86*, 889–903. [CrossRef]
39. Nieß, S.; Armbruster, U.; Dietrich, S.; Klemm, M. Recent advances in catalysis for methanation of CO_2 from biogas. *Catalysts.* **2022**, *12*, 374. [CrossRef]
40. Gaikwad, R.; Villadsen, S.N.B.; Rasmussen, J.P.; Grumsen, F.B.; Nielsen, L.P.; Gildert, G.; Møller, P.; Fosbøl, F.L. Container-sized CO_2 to methane: Design, construction and catalytic tests using raw biogas to biomethane. *Catalysts* **2020**, *10*, 1428. [CrossRef]
41. Aragüés-Aldea, P.; Sanz-Martínez, A.; Durán, P.; Francés, E.; Peña, J.A.; Herguido, J. Improving CO_2 methanation performance by distributed feeding in a Ni-Mn catalyst fixed bed reactor. *Fuel* **2022**, *321*, 124075. [CrossRef]
42. Zhou, L.; Li, L.; Wei, N.; Li, J.; Basset, J.-M. Effect of $NiAl_2O_4$ formation on Ni/Al_2O_3 stability during Dry Reforming of Methane. *ChemCatChem* **2015**, *7*, 2508–2516. [CrossRef]
43. Chen, L.; Li, Y.; Zhang, X.; Zhang, Q.; Wang, T.; Ma, L. Effect of Ru particle size on hydrogenation/decarbonylation of propanoic acid over supported Ru catalysts in aqueous phase. *Catal. Lett.* **2017**, *147*, 29–38. [CrossRef]
44. Burger, T.; Augenstein, H.M.S.; Hnyk, F.; Döblinger, M.; Köhler, K.; Hinrichsen, O. Targeted Fe-doping of Ni-Al catalysts via the surface redox reaction technique for unravelling its promoter effect in the CO_2 methanation reaction. *ChemCatChem* **2020**, *12*, 649–662. [CrossRef]
45. Jürgensen, L.; Ehimen, E.A.; Born, J.; Holm-Nielsen, J.B. Dynamic biogas upgrading based on the Sabatier process: Thermodynamic and dynamic process simulation. *Bioresour. Technol.* **2015**, *178*, 323–329. [CrossRef] [PubMed]
46. Cárdenas-Arenas, A.; Quindimil, A.; Davó-Quiñonero, A.; Bailón-García, E.; Lozano-Castelló, D.; De-La-Torre, U.; Pereda-Ayo, B.; González-Marcos, J.A.; González-Velasco, J.R.; Bueno-López, A. Isotopic and in situ DRIFTS study of the CO_2 methanation mechanism using Ni/CeO_2 and Ni/Al_2O_3 catalysts. *Appl. Catal. B Environ.* **2020**, *265*, 118538. [CrossRef]
47. Durán, P.; Esteban, I.; Francés, E.; Herguido, J.; Peña, J.A. CO_2 methanation using Ru based catalysts for storage and distribution of energy: Activation of catalyst strategies. In Proceedings of the European Hydrogen Energy Conference (EHEC), Malaga, Spain, 14–16 March 2018; pp. 243–244.
48. Garbarino, G.; Bellotti, D.; Riani, P.; Magistri, L.; Busca, G. Methanation of carbon dioxide on Ru/Al_2O_3 and Ni/ Al_2O_3 catalysts at atmospheric pressure: Catalysts activation, behaviour and stability. *Int. J. Hydrogen Energy* **2015**, *40*, 9171–9182. [CrossRef]